Molecular Cell, Volume *78*

Supplemental Information

Lamina-Dependent Stretching and Unconventional Chromosome Compartments in Early *C. elegans* Embryos

Ahilya N. Sawh, Maxwell E.R. Shafer, Jun-Han Su, Xiaowei Zhuang, Siyuan Wang, and Susan E. Mango

Supplemental Information:

Figures S1 to S7

Supplemental Figure legends:

Figure S1. Related to Figure 1.

Marker-based volumetric image segmentation separates chromosome territories.
Given the proximity of multiple nuclei within an embryo, we developed methods to constrain chromosome tracing to within the volumes of individual chromosome territories. (A) Z-Slices of individual nuclear volumes identified by watershed algorithm based on a general DNA stain. Z-stack positions are relative to the entire embryo, same sample as in Figure 1. Each nucleus identified is colored differently. (B) Similar segmentation as in (A) of the Figure 1 embryo, but using the primary probe reconstruction as the marker for individual chromosome territories. Each volume of contiguous primary probe signal identified is colored differently. Chromosome tracing was restricted to these individual territories to separate TADs belonging to different chrV copies. This method assumes a given TAD probe belongs within its surrounding primary probe volume. (C) Bar graph of the number of measurements made for each of the 231 chrV TAD pairs.

Figure S2. Related to Figure 2.

Long-range interactions drive eigenvector-based compartment calls.
(A) To test the robustness of chrV measurements, we asked if down-sampling of data would generate similar chromosome conformation matrices. Mean pairwise distance matrices (μm) produced after down-sampling the total traces two-fold in six independent iterations. In all iterations, chromosome arms are separated in space, indicating this finding is robust. (B) (left) Distance matrix of early embryos (2-40cells), same as Figure 2A. (middle) Eigenvector decomposition of the distance matrix. The PC1 profile is similar to pre-gastrula embryos and not post-gastrula embryos. (right) Each TAD from the distance matrix is plotted in 2D principal component space. Compartment calls are presented as white/gray/black bars. TADs with similar pairwise distance patterns are labeled by shape (**O**, □, x). (C-D) (left) Toy datasets where long-range interactions were modulated (within dotted green boxes): to increase interactions between the arms in the early embryo spatial distance matrix (C) or remove long-range interactions in the late embryo matrix (D). (middle) Standard

eigenvector decomposition on the toy data, showing changes in long-range interactions between the arms drive the PC1 profile. (right) Each TAD from the inter-TAD matrix is plotted in 2D principal component space. (E) Difference matrix detailing changes that occur in chrV structure during early embryonic development, in µm (gastrula structure – pre-gastrula structure). Significance calculated by one-way Anova for each pairwise distance at the different stages. All significant changes were through compaction (red) and predominantly long-range, regions in white had no significant change. (F) Schematic representation of chrV compartment-level structure over embryogenesis. Pre-gastrula chromosomes have unconventional compartmentalization (a single A compartment and two separated B compartments), requiring multidimensional analysis for accurate classification. After the onset of gastrulation, chrV displays conventional compartmentalization of a single A compartment and a unified B compartment. PC1 distinguishes the A from the B compartment TADs in conventional compartmentalization because the two arms are close in space.

Figure S3. Related to Figure 2.

Whole chromosome I tracing by multiplexed FISH.

(A) Schematic of chrI annotated with TAD boundaries (orange ticks) and FISH probe positions (colored dots 1-14). (B) Example of raw data z-projections on a ~14-cell embryo of each hybridization round. Scale bar = 5 µm. (bottom) Bar graph of the number of measurements made for each of the 91 chrI TAD pairs. (C) Distance matrix of chrI in early embryos (2-40cells). (D) Normalized distance matrix, plotted as observed spatial distance as a function of genomic distance for each TAD pair. Red denotes pairs that are closer than expected, blue the opposite. (E) Eigenvector decomposition of the distance matrix. The early embryo PC1 profile for chrI is similar to the early embryo chrV profile, where the arms have opposing signs. ChrI lacks conventional compartmentalization. (Figure S2B, Figure 2E).

Figure S4. Related to Figure 4.

ChrI compacts upon loss of *cec-4*.

(A) (top) ChIP-seq signal for LEM-2 (lamina association) across chrI, plotted as z-score of ChIP-input for two replicates (blue lines). (bottom) Z-score difference (*cec-4* – wild-type) of LEM-2 ChIP, average of 2 replicates. Regions in red indicate loss of lamina association in the mutant. Data from (Gonzalez-Sandoval et al., 2015). (B) Mean

distance matrix between chrI TADs in *cec-4* mutants. (C) TAD-specific changes in normalized mean distance from wild-type to *cec-4* embryos. LADs are displayed in purple bars.

Figure S5. Related to Figure 5.

ChrV chromosome clusters show distinct markers of variation and spatial organization. (A) As an alternative visual representation of the chromosome clusters we performed *t*-SNE dimensionality reduction and plotted the traces in 2D tSNE space. (B) As a control, we re-colored the *t*SNE plot in (A) according to the biological replicate experiment where each trace originated. A single biological experiment captured many individual chromosome traces. Individual experiments do not show clustering patterns similar to those in Figure 4A, confirming the clusters are not due to biological batch effects. (C) Radii of gyration of individual wild-type chromosomes in the total population and each cluster, indicating cluster δ contains the largest conformations. Data presented by raincloud plot, as in Figure 3. (D) TAD-TAD unique markers of variation were identified by Wilcoxon test in Seurat (Butler et al., 2018). For each cluster, white-filled boxes represents a TAD pairs that was different (closer or farther) than the chromosomes in all the other clusters. Black-filled boxes represent TAD pairs that were not uniquely different. Cluster α markers were concentrated in the left half of the chromosome, Cluster β markers in the right half, and Cluster γ markers in the long-distance pairs between the arms. Cluster δ (most dissimilar from the average) showed markers of variation throughout the chromosome. (E) PC1 profiles of chromosomes in each cluster, as in Figure 2. The profile of Cluster γ most closely resembles conventional compartmentalization. (F) Example chromosome traces from each cluster. TADs of the left (blue) and right (red) arms are enclosed in 3D Delaunay triangulations to visualize their occupied volumes. (G) Polarization index of left and right arm volumes in individual chromosomes by cluster. Points are jittered for visualization purposes. Almost all chromosome arms do not share any volume (polarization = 1), indicating the left and right B compartments do not intermingle extensively. (H) Histograms with kernel distribution fits of distances between arm centroids of individual chromosomes, showing different distributions of distances between sub-populations.

Figure S6. Related to Figure 6.

ChrI displays prevalent structural heterogeneity in early embryos.

(A) UMAP plot of five chrI clusters, where each dot is a single trace. Clusters 0 and 1 appear intermingled in UMAP space. (B) UMAP plot of clusters 2-3-4, to aid in visualization. (C) Mean distance matrices chrI sub-populations (clusters 0-4). (D) Normalized mean distance matrices for each cluster as observed/expected values. Compartment calls are presented as white/gray/black bars, as in Figure 2. Cluster 2 displays conventional compartmentalization. (E) Power-law scaling of mean spatial distance versus genomic distance for each chrI cluster (blue, best fit curves of the raw data). *s* = scaling exponent of spatial distance, *a* = step size. Values in brackets are 95% confidence intervals of the fit. Dotted line: fractal globule polymer model prediction with *s* = 1/3. Cluster 4 displays a folding pattern similar to the fractal globule.

Figure S7. Related to Figure 7.

ChrI *cec-4* chromosome clusters are more compact and disorganized than wild-type. (A) *t*-SNE plot comparing chrI wild-type (blue) and *cec-4* (red) chromosome traces (left). UMAP plot of chrI *cec-4* clusters (right). (B) Mean distance matrices *cec-4* sub-populations (clusters 0-2). (C) Difference matrices between each *cec-4* cluster and the wild-type population average (red indicates compaction, blue separation). (D) Normalized mean distance matrices for each cluster as observed/expected values. Compartment calls are presented as white/gray/black bars, as in Figure 2. No cluster displays conventional compartmentalization, cluster 1 and 2 are highly disorganized.

Sawh et al. FIGURE S1
related to Figure 1

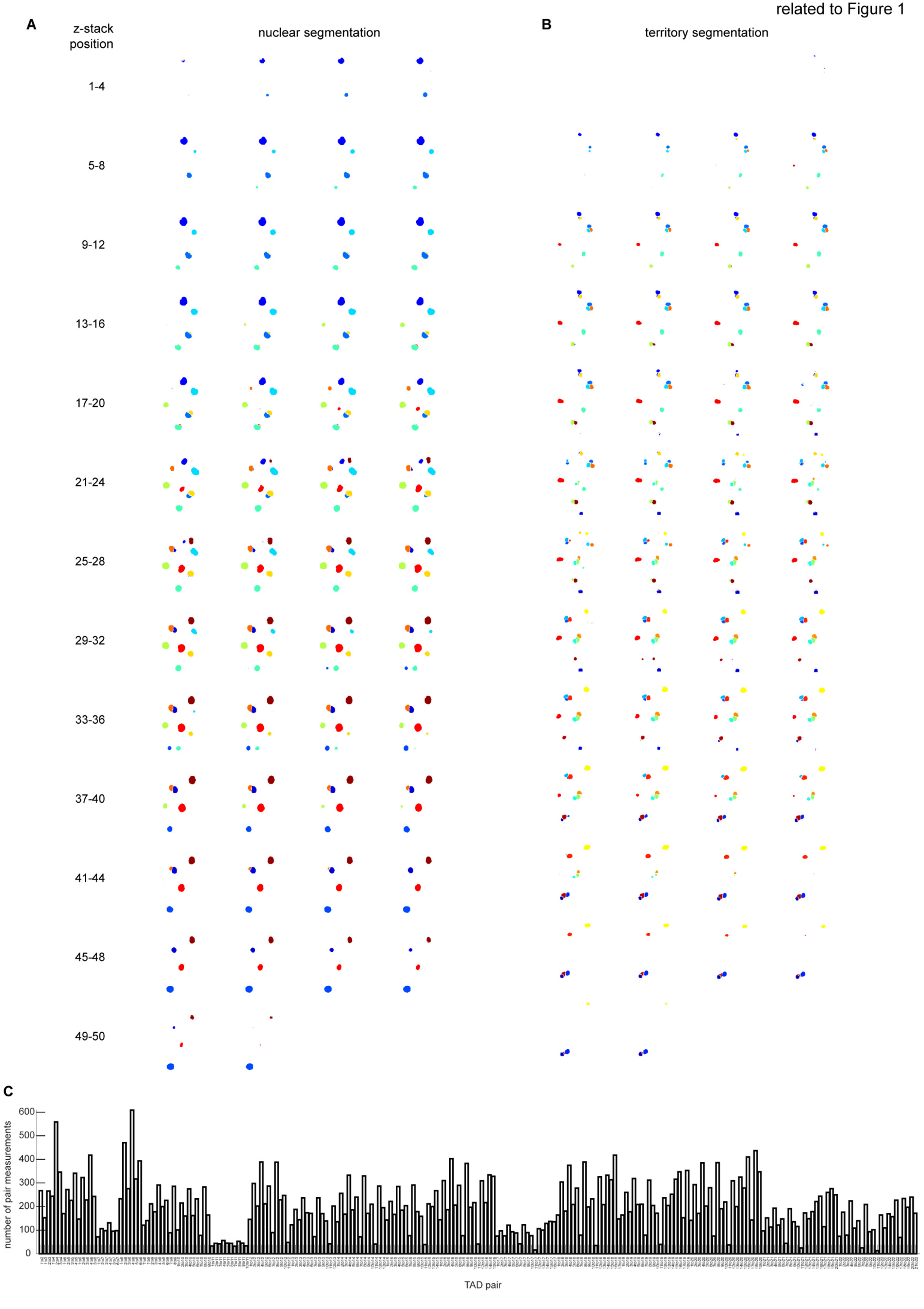

Sawh et al. FIGURE S2
related to Figure 2

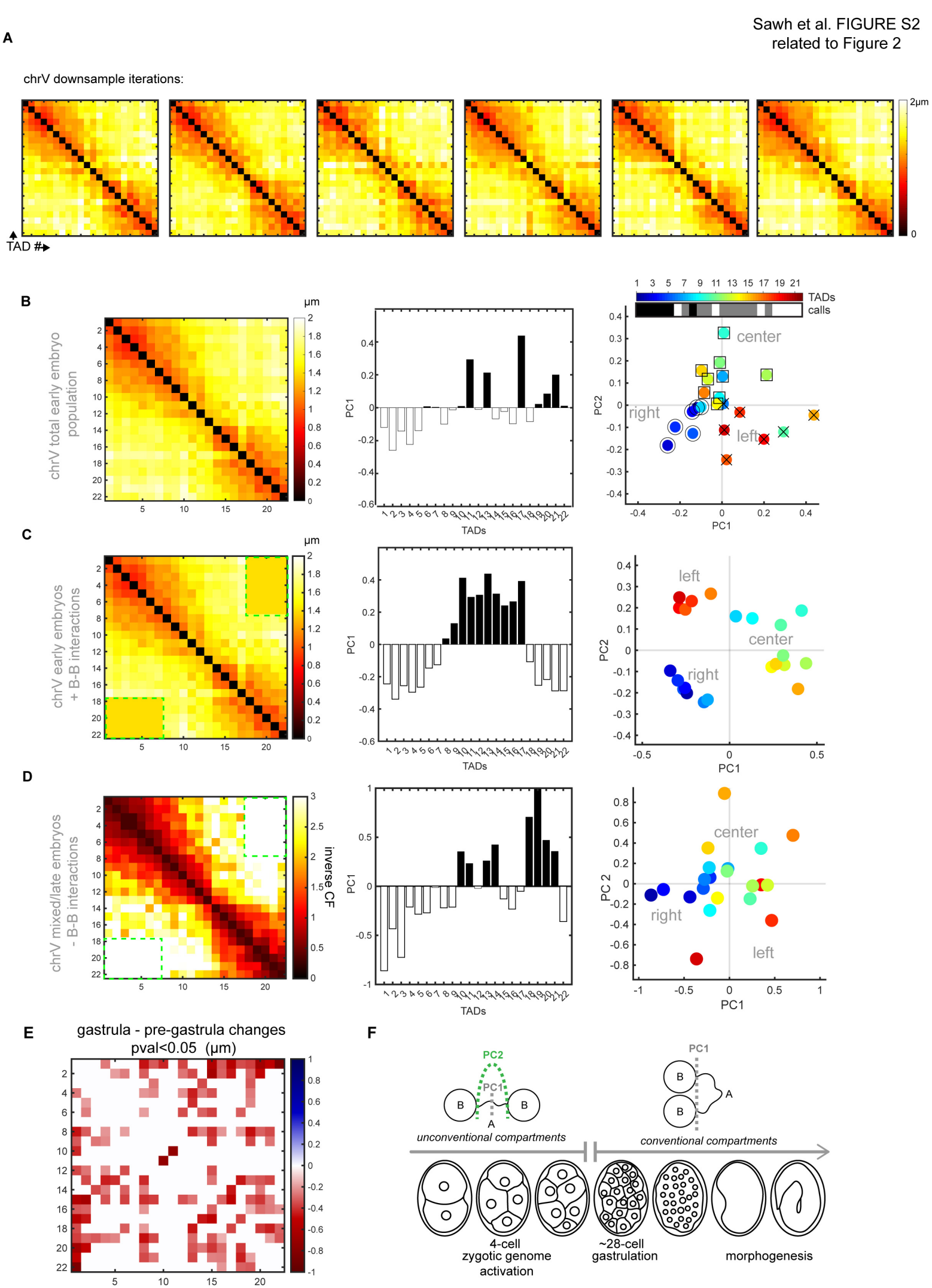

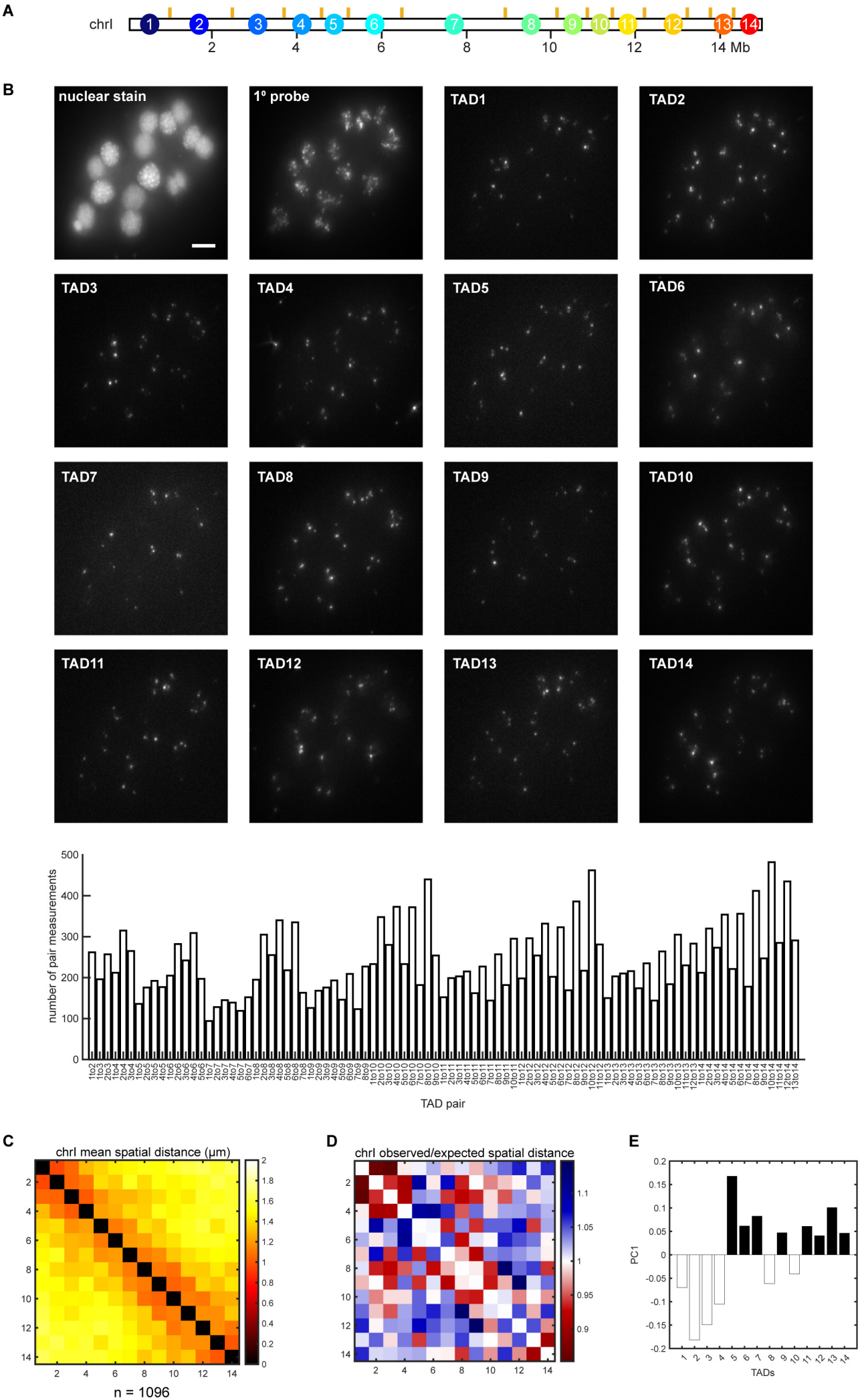
A
chrI
1
2
3
4
5
6
7
8
9
10
11
12
13
14
2
4
6
8
10
12
14 Mb
B
nuclear stain
1º probe
TAD1
TAD2
TAD3
TAD4
TAD5
TAD6
TAD7
TAD8
TAD9
TAD10
TAD11
TAD12
TAD13
TAD14
number of pair measurements
0
100
200
300
400
500
TAD pair
C
chrI mean spatial distance (μm)
n = 1096
D
chrI observed/expected spatial distance
E
PC1
TADs

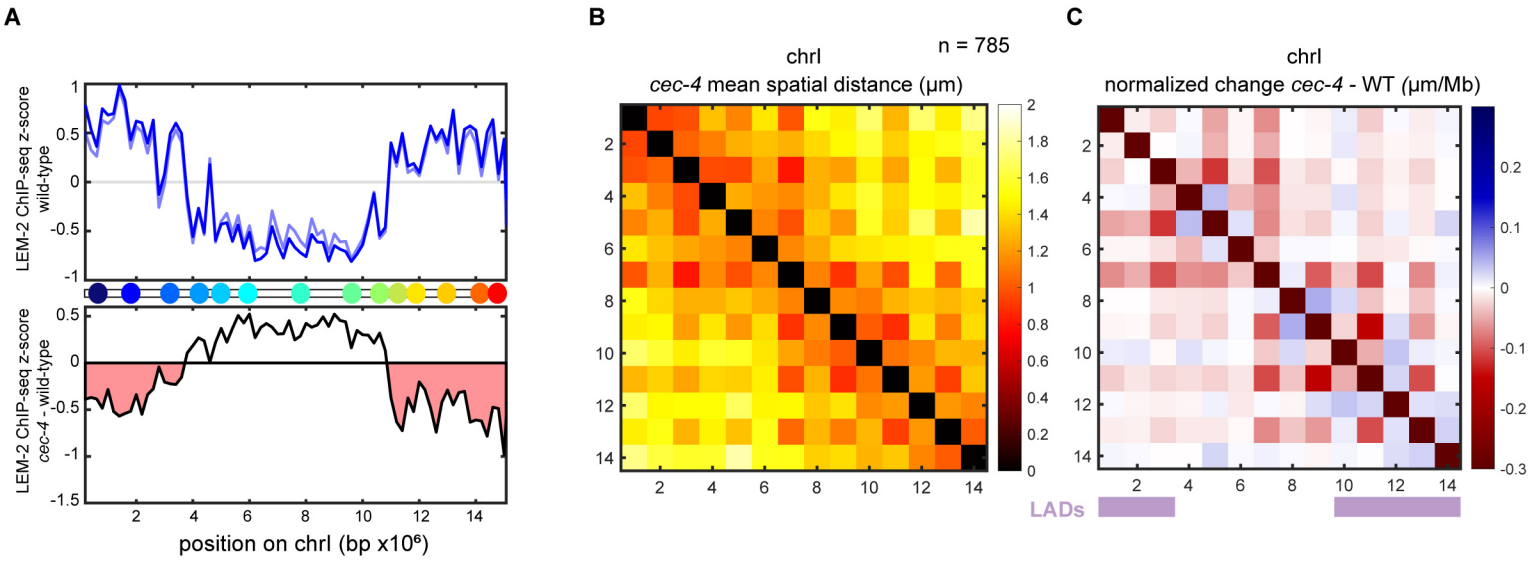
A
LEM-2 ChIP-seq z-score
wild-type
LEM-2 ChIP-seq z-score
cec-4 - wild-type
position on chrI (bp x10⁶)
B
chrI
n = 785
cec-4 mean spatial distance (µm)
C
chrI
normalized change cec-4 - WT (µm/Mb)
LADs

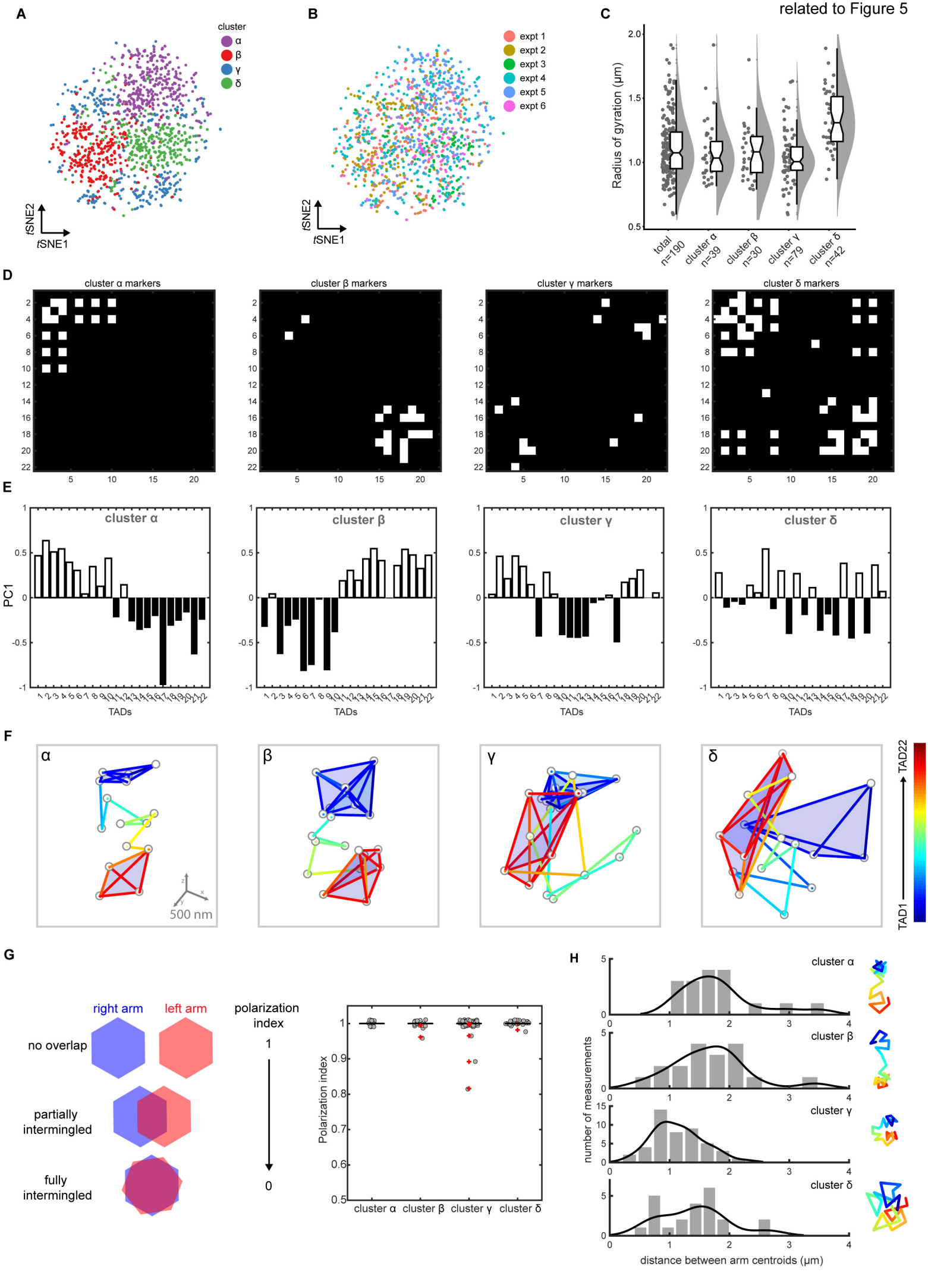
A
cluster
α
β
γ
δ
tSNE2
tSNE1
B
expt 1
expt 2
expt 3
expt 4
expt 5
expt 6
tSNE2
tSNE1
C
Radius of gyration (μm)
2.0
1.5
1.0
0.5
total n=190
cluster α n=39
cluster β n=30
cluster γ n=79
cluster δ n=42
D
cluster α markers
cluster β markers
cluster γ markers
cluster δ markers
E
cluster α
cluster β
cluster γ
cluster δ
PC1
TADs
F
α
β
γ
δ
500 nm
TAD22
TAD1
G
right arm
left arm
no overlap
partially intermingled
fully intermingled
polarization index
1
0
Polarization index
cluster α
cluster β
cluster γ
cluster δ
H
cluster α
cluster β
cluster γ
cluster δ
number of measurements
distance between arm centroids (μm)

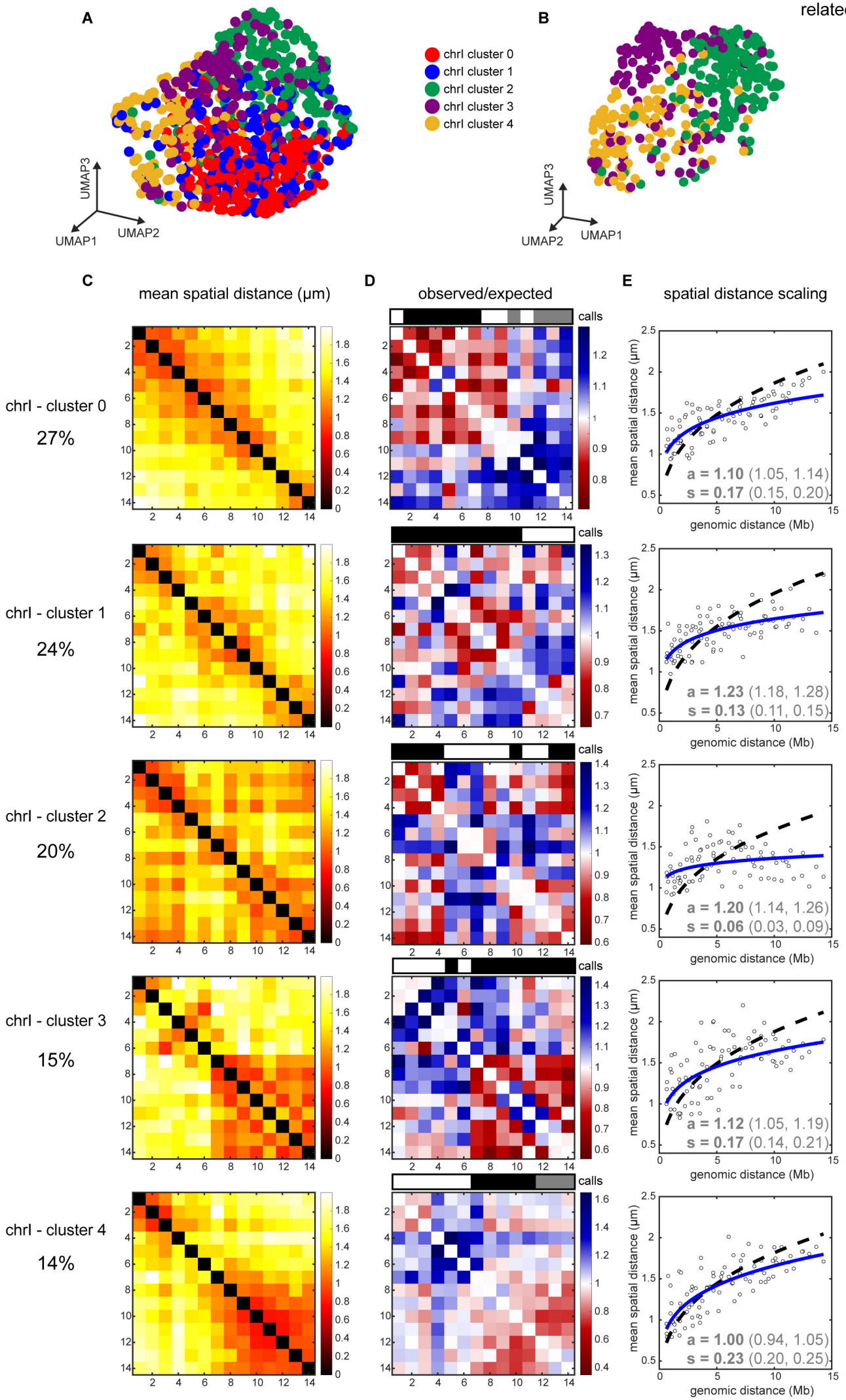
A
B
chrl cluster 0
chrl cluster 1
chrl cluster 2
chrl cluster 3
chrl cluster 4
UMAP3
UMAP1
UMAP2
UMAP3
UMAP2
UMAP1
C
mean spatial distance (μm)
D
observed/expected
E
spatial distance scaling
calls
mean spatial distance (μm)
genomic distance (Mb)
chrl - cluster 0
27%
a = 1.10 (1.05, 1.14)
s = 0.17 (0.15, 0.20)
chrl - cluster 1
24%
a = 1.23 (1.18, 1.28)
s = 0.13 (0.11, 0.15)
chrl - cluster 2
20%
a = 1.20 (1.14, 1.26)
s = 0.06 (0.03, 0.09)
chrl - cluster 3
15%
a = 1.12 (1.05, 1.19)
s = 0.17 (0.14, 0.21)
chrl - cluster 4
14%
a = 1.00 (0.94, 1.05)
s = 0.23 (0.20, 0.25)

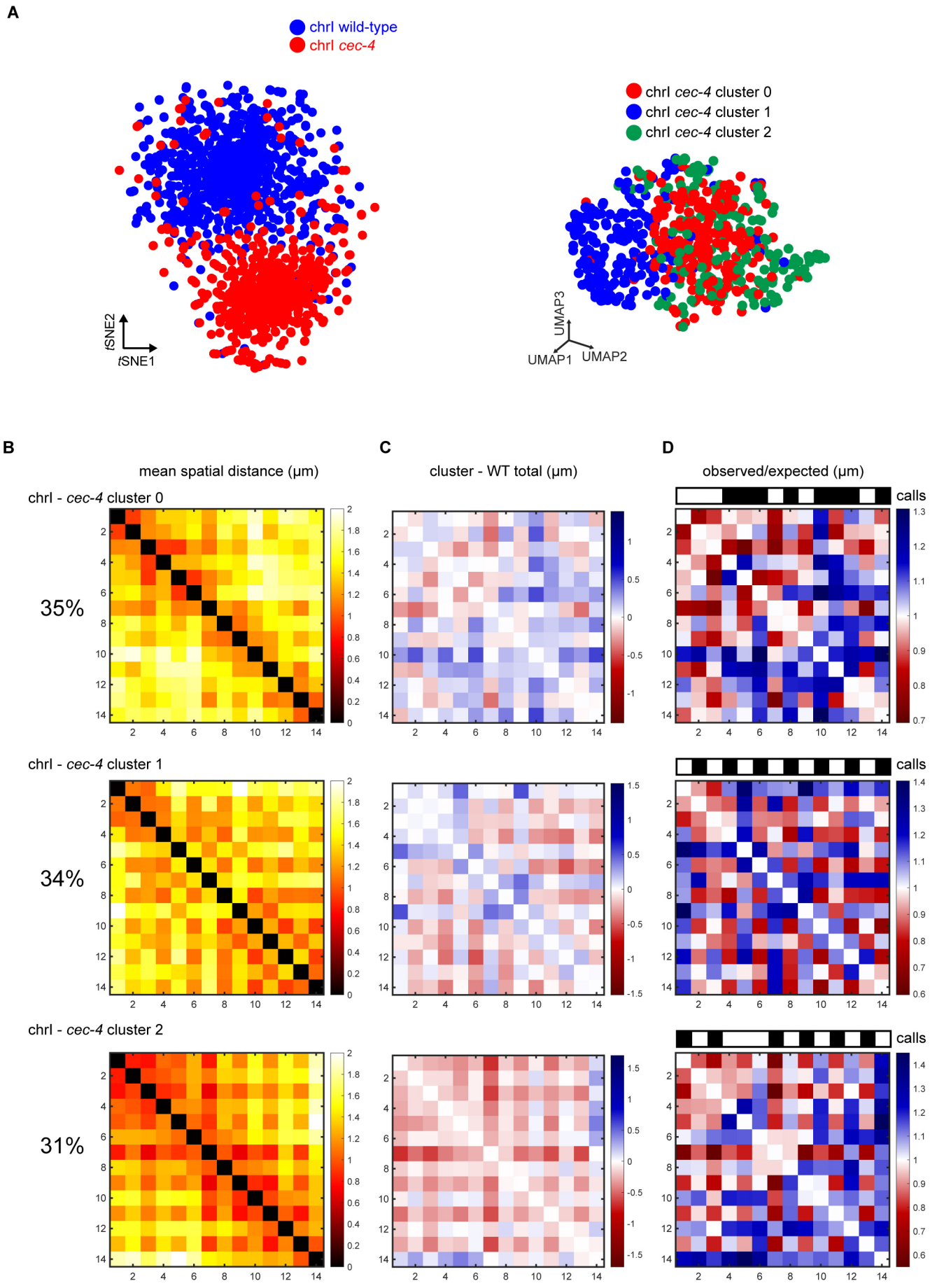
A
chrI wild-type
chrI cec-4
tSNE2
tSNE1
chrI cec-4 cluster 0
chrI cec-4 cluster 1
chrI cec-4 cluster 2
UMAP3
UMAP1
UMAP2
B
mean spatial distance (µm)
C
cluster - WT total (µm)
D
observed/expected (µm)
calls
chrI - cec-4 cluster 0
35%
chrI - cec-4 cluster 1
34%
chrI - cec-4 cluster 2
31%